Characterization and functional analysis of *Toxoplasma* Golgi-associated proteins identified by proximity labelling

Authors:

Rebecca R. Pasquarelli[1], Justin J. Quan[2], Emily S. Cheng[2], Vivian Yang[1], Timmie A. Britton[1], Jihui Sha[3], James A. Wohlschlegel[3], and Peter J. Bradley[1,3*]

[1]Molecular Biology Institute, University of California, Los Angeles, CA 90095, USA

[2]Department of Microbiology, Immunology, and Molecular Genetics, University of California, Los Angeles, CA 90095, USA

[3]Department of Biological Chemistry and Institute of Genomics and Proteomics, University of California, Los Angeles, California, USA

Running head: Characterization of *Toxoplasma* Golgi proteins

* Corresponding author: pbradley@ucla.edu, tel. 310-825-8386, fax 310-825-5231

Abstract

Toxoplasma gondii possesses a highly polarized secretory pathway that contains both broadly conserved eukaryotic organelles and unique apicomplexan organelles which play essential roles in the parasite's lytic cycle. As in other eukaryotes, the *T. gondii* Golgi apparatus sorts and modifies proteins prior to their distribution to downstream organelles. Many of the typical trafficking factors found involved in these processes are missing from apicomplexan genomes, suggesting that these parasites have evolved unique proteins to fill these roles. Here we identify a novel Golgi-localizing protein (ULP1) which contains structural homology to the eukaryotic trafficking factor p115/Uso1. We demonstrate that depletion of ULP1 leads to a dramatic reduction in parasite fitness and replicative ability. Using ULP1 as bait for TurboID proximity labelling and immunoprecipitation, we identify eleven more novel Golgi-associated proteins and demonstrate that ULP1 interacts with the *T. gondii* COG complex. These proteins include both conserved trafficking factors and parasite-specific proteins. Using a conditional knockdown approach, we assess the effect of each of these eleven proteins on parasite fitness. Together, this work reveals a diverse set of novel *T. gondii* Golgi-associated proteins that play distinct roles in the secretory pathway. As several of these proteins are absent outside of the Apicomplexa, they represent potential targets for the development of novel therapeutics against these parasites.

40 **Importance**

41 Apicomplexan parasites such as *Toxoplasma gondii* infect a large percentage of
42 the world's population and cause substantial human disease. These widespread
43 pathogens use specialized secretory organelles to infect their host cells, modulate host
44 cell functions, and cause disease. While the functions of the secretory organelles are now
45 better understood, the Golgi apparatus of the parasite remains largely unexplored,
46 particularly regarding parasite-specific innovations that may help direct traffic
47 intracellularly. In this work, we characterize ULP1, a protein that is unique to parasites but
48 shares structural similarity to the eukaryotic trafficking factor p115/Uso1. We show that
49 ULP1 plays an important role in parasite replication and demonstrate that it interacts with
50 the conserved oligomeric Golgi (COG) complex. We then use ULP1 proximity labelling to
51 identify eleven additional Golgi-associated proteins which we functionally analyze via
52 conditional knockdown. This work expands our knowledge of the *Toxoplasma* Golgi
53 apparatus and identifies potential targets for therapeutic intervention.

54

55

56 **Introduction**

57 *Toxoplasma gondii* is an obligate intracellular parasite in the phylum Apicomplexa.
58 This phylum includes parasites of both human and veterinary medical importance
59 including *Plasmodium spp*. (malaria), *Cryptosporidium spp*. (diarrheal disease), *Eimeria*
60 *spp*. (chicken coccidiosis), and *Neospora caninum* (neosporosis) (1–5). Approximately
61 one-third of the global human population is chronically infected with *T. gondii* (6). While
62 infection is usually asymptomatic in healthy individuals, the parasite can cause severe or
63 fatal disease in immunocompromised people and congenitally infected neonates (7–9).
64 While treatments exist that can suppress the acute infection, they are unable to clear the
65 parasite completely resulting in lifelong chronic infection (8). A deeper understanding of
66 apicomplexan biology is needed to inform the discovery of novel parasite-specific
67 therapeutics.

68 Apicomplexan parasites possess a unique and highly polarized secretory pathway
69 which plays an essential role in their life cycles (10,11). The endomembrane system of
70 these parasites includes the endoplasmic reticulum and a Golgi apparatus, which is
71 composed of a single stack of three to five cisternae, as well as several apicomplexan-
72 specific organelles including the rhoptries, micronemes, dense granules, and inner
73 membrane complex (IMC) (12,13). During parasite replication, these organelles are
74 formed de novo from vesicles which bud from the Golgi and are trafficked through the
75 secretory pathway to their destinations (14). The secretory pathway also delivers cargo to
76 the plant-like vacuole (PLVAC), endosome like compartment (ELC), and a non-
77 photosynthetic plastid called the apicoplast (15–18). As each of these organelles are
78 essential, correct protein sorting is important for the survival of the parasite.

79 Recent studies have revealed a surprising intersection between *T. gondii*'s
80 endocytic and exocytic pathways. Several Rabs which are components of the endosomal
81 system in most eukaryotes, such as Rab5a and Rab7, have instead been repurposed as

82 secretory trafficking proteins that reside in the ELC. The PLVAC, a hydrolytic compartment
83 analogous to the lysosome, has been implicated in multiple roles such as autophagy,
84 degradation of host-derived proteins, and proteolytic processing of proteins that are
85 trafficked to the micronemes and rhoptries (16,19,20). Disruption of proteins that localize
86 to the PLVAC and ELC or proteins that are typically involved in endosomal trafficking has
87 been shown to cause defects in the biogenesis of rhoptries and micronemes (11,16,21–
88 23). Furthermore, endolysosomal proteases have been shown to proteolytically process
89 immature ROP and MIC proteins (16,19,20). Together, this evidence supports the
90 convergence of endocytic and exocytic pathways in *T. gondii*.

91 Several key trafficking factors that play critical roles in protein trafficking in most
92 eukaryotes are missing in apicomplexan genomes. Specifically, *T. gondii* and other
93 apicomplexans lack most components of the Endosomal Sorting Complexes Required for
94 Transport (ESCRT) and the Golgi-localized Gamma adaptin ear-containing ARF-binding
95 (GGA) proteins (11,24,25). This limited repertoire of classical protein trafficking machinery
96 suggests that apicomplexans may have evolved their own specialized proteins and
97 pathways to facilitate these functions. Here we report the identification of a novel parasite-
98 specific Golgi protein, ULP1, which is structurally homologous to the eukaryotic tethering
99 factor p115/Uso1. We show that ULP1 plays a critical role in parasite fitness and its
100 depletion results in defective parasite replication. We then use TurboID proximity labelling
101 and immunoprecipitation to show that ULP1 interacts with the *T. gondii* conserved
102 oligomeric Golgi (COG) complex and identify eleven previously uncharacterized Golgi-
103 associated proteins. Finally, we analyze the orthology of each novel protein and use a
104 conditional knockdown approach to assess their impact on parasite fitness, revealing
105 several essential proteins and several more parasite-specific proteins.
106
107

108 **Results**

109

110 **TGGT1_289120 is a parasite-specific Golgi protein that is important for parasite**
111 **fitness**

112 We identified a 290 kDa hypothetical protein with the gene ID TGGT1_289120
113 during our previous proximity labelling experiments using IMC proteins as bait (26).
114 BLASTp analysis revealed that TGGT1_289120 has orthologs in *Hammondia*, *Neospora*,
115 *Besnoitia, Cystoisospora*, and *Sarcocystis* but appears to be absent from other
116 apicomplexan parasites and higher eukaryotes (27). Secondary structure analysis using
117 Phyre2 revealed that residues 495-647 of TGGT1_289120 contain structural homology to
118 the globular head domain of p115/Uso1, a membrane tethering protein conserved in
119 eukaryotes (28,29). InterPro also identified an armadillo (ARM)-like domain within this
120 region, and DeepCoil2 predicted a coiled-coil (CC) domain within residues 1736-1812 (Fig
121 1A) (30,31). p115/Uso1 also contains ARM repeats within its globular head domain and a
122 single CC domain near the C-terminus, further supporting their structural similarity (29).
123 While this study was being prepared for publication, a study of the *T. gondii* COG complex
124 by Marsilia et al. independently identified TGGT1_289120 and named it Uso1-like protein
125 1 (TgULP1) based on its structural similarity to the p115/Uso1 protein (32). To maintain
126 consistency, we adopted the same nomenclature and also named the protein ULP1.

127 The similarity to the essential vesicular trafficking factor p115/Uso1 and its low
128 phenotype score of -3.8 in a genome wide CRISPR/Cas9 screen (GWCS) led us to
129 hypothesize that this protein may play a key role in secretory trafficking in *T. gondii* (33).
130 To determine the localization of ULP1, we used CRISPR/Cas9 to fuse sequences
131 encoding a C-terminal 3xHA epitope tag at its endogenous locus (34,35).
132 Immunofluorescence assay (IFA) revealed that ULP1 localized to a distinct bar-shaped
133 region anterior to the nucleus, suggesting localization to the Golgi apparatus. To confirm

134 this, we co-stained for GRASP55-YFP, a marker of the cis-medial Golgi apparatus in *T.*
135 *gondii* and found that the two proteins colocalized (Fig 1B) (36).

136 To study the function of ULP1, we used the auxin-inducible degron (AID) system
137 which allows rapid proteasomal degradation of a target protein upon treatment with
138 indoleacetic acid (IAA) (37,38). To create an ULP1^{AID} parasite strain, we fused sequences
139 encoding an mAID-3xHA tag to the 3' end of the gene in a strain that carries the TIR1
140 auxin-receptor FBOX protein. IFA showed that the degron-tagged protein localizes
141 appropriately and is completely depleted after 24 hours of IAA treatment (Fig 1C). The
142 ULP1-depleted parasites did not appear to exhibit defects in overall morphology. To
143 assess how loss of ULP1 would affect the parasite's overall lytic ability, we performed
144 plaque assays, which showed a dramatic 88.7% decrease in plaque size when ULP1 was
145 depleted (Fig 1D, E). To determine whether this defect in lytic ability was due to defects in
146 replication, we quantified the number of parasites per vacuole after 30 hours of growth for
147 parasites treated with IAA or a vehicle control. At 30 hours post-infection, ULP1-depleted
148 parasites were found primarily in 8-parasite vacuoles, whereas untreated parasites were
149 primarily found in 16-parasite vacuoles (Fig 2F). This indicates that the defect in overall
150 lytic ability is due to a defect in replication. Given the low phenotype score (-3.8), we
151 wondered whether the slow growth and ability to form small plaques may be due to some
152 residual ULP1 which escaped degradation. To determine if this was the case, we used
153 CRISPR/Cas9 to disrupt the endogenous locus for ULP1 and verified loss of the protein
154 by both IFA and PCR (Fig 1G-H). Using this method, we successfully generated a Δ*ulp1*
155 strain which phenocopied the plaque defect exhibited by IAA-treated ULP1^{AID} parasites
156 (Fig 1I-J). To avoid potential issues with functional compensation, which has been
157 previously documented for knockout strains in *T. gondii*, we decided to proceed with the
158 ULP1^{AID} strain for further phenotypic analysis (39–41).

159 Next, we used IFA to assess whether depletion of ULP1 resulted in aberrant
160 organellar morphology. We began by endogenously tagging the known Golgi protein
161 TgTrs85 to determine whether loss of ULP1 would affect the Golgi apparatus (18). When
162 we depleted ULP1, we found that TgTrs85 was unaffected (Fig 2A). We next stained for
163 DrpB, a dynamin-related protein that localizes to post-Golgi vesicles, which also appeared
164 to be unaffected (Fig 2B) (23). Other components of the secretory pathway such as the
165 PLVAC (marked by NHE3), endoplasmic reticulum (SERCA), and ELC (Vps9) were
166 similarly unaffected (Fig 2C-E). Next, we wanted to determine whether the morphology of
167 downstream secretory organelles was altered, so we stained for the rhoptries (ROP7),
168 micronemes (MIC2), and dense granules (GRA14). We additionally stained for the
169 apicoplast (Atrx1) and mitochondrion (F1β ATPase). Surprisingly, we did not observe
170 mislocalization of any of these markers, indicating these organelles are not grossly
171 affected upon ULP1 knockdown (Fig 2F-J).
172
173 **ULP1 proximity labelling and immunoprecipitation yields candidate Golgi proteins**
174 To identify additional novel Golgi proteins, we decided to use ULP1 as bait for both
175 proximity labeling and immunoprecipitation (IP) experiments. For proximity labelling, the
176 biotin ligase TurboID-3xHA was fused to the C-terminus of ULP1 (Fig 3A) (42). The
177 ULP1^{TurboID} fusion protein was detectable by IFA and trafficked appropriately to the Golgi
178 apparatus. In the absence of biotin, only the endogenously biotinylated apicoplast stained
179 with streptavidin. Upon addition of biotin, the Golgi apparatus also stained with
180 streptavidin, confirming that the ULP1^{TurboID} fusion protein was enzymatically active and
181 biotinylated proximal Golgi proteins (Fig 3B). Western blot analysis confirmed that the
182 addition of biotin resulted in dramatically increased amounts of biotinylated proteins in
183 ULP1^{TurboID} lysates (Fig 3C). The IP analysis was performed on the ULP1^{3xHA} strain.
184 Western blot showed that the 3xHA-tagged protein migrated at a smaller size than

185 expected based on its molecular weight of 290 kDa and exhibited significant protein
186 breakdown. During the process of affinity chromatography for the IP experiment, the
187 protein experienced even more severe breakdown. Despite this, the elution fraction was
188 still highly enriched for the HA-tagged protein (Fig 3D). Thus, we continued with the
189 experiment.

190 As expected, the bait protein ULP1 was the top hit identified by mass spectrometry
191 in the IP experiments and was among the top 5 hits in the TurboID experiment (Table S1
192 and Table S2). DrpB, TgTrs85, TgEpsL, and Vps9, which have all been previously shown
193 to localize to the *Toxoplasma* Golgi apparatus or nearby compartments of the secretory
194 pathway, were highly enriched in our TurboID experiment (Table S1) (18,23,43,44). In
195 addition, many of the top hits are predicted to be involved in processes such as ER-to-
196 Golgi retrograde transport, Golgi organization, and intracellular protein transport. Many of
197 the most enriched proteins were hypothetical proteins that have not previously been
198 studied. Domain analysis allowed us to identify two of these hypothetical proteins,
199 TGGT1_278890 and TGGT1_262450, as homologs of the known Golgi proteins CDP/cut
200 alternatively spliced product (CASP) and dymeclin (DYM), respectively.

201 Our IP experiment identified several interesting candidate interactors, including the
202 hypothetical protein TGGT1_216370, which was also among the top hits in the TurboID
203 experiment (Table S2). In addition, homologs of all eight subunits of the COG complex
204 immunoprecipitated with ULP1 and were highly enriched in our TurboID experiment. All
205 eight are currently annotated as hypothetical proteins, but BLASTp and functional domain
206 analysis supports their designation as COG complex subunits, although the BLASTp e-
207 value for COG1 is weak (e^{-6}) (24). As p115/Uso1 is a known interactor of the COG complex
208 via direct binding to COG2, this result further supports the designation of ULP1 as a
209 p115/Uso1-like protein (45). Several additional proteins were found to immunoprecipitate
210 with ULP1, although fewer peptides were recovered for these proteins. Among these lower

211 abundance hits were a Sec23/Sec24 trunk domain-containing protein, TgEpsL, COP1
212 subunit ε, the cyclin-dependent kinase (CDK)-related kinase Crk2, Vps35, Rab7, AP1-γ,
213 and DrpB.
214
215 **Verification of candidate Golgi proteins**
216 To continue our study of the *Toxoplasma* Golgi apparatus, we selected eleven
217 uncharacterized proteins with GWCS phenotype scores of less than -2 from our TurboID
218 and IP hits (Table 1). Candidates were prioritized based on functional domain analysis
219 and orthology to known Golgi proteins. Five of the selected genes appeared to be direct
220 orthologs of known Golgi-associated proteins. TGGT1_290310 is the putative COG1
221 orthologue that we identified in our ULP1 IP. TGGT1_311400 is annotated as WD domain,
222 G-beta repeat-containing protein, but BLASTp analysis revealed its identity as Sec31.
223 TGGT1_232190 contains a Sec7 domain within a larger Golgi Brefeldin A resistance
224 guanine nucleotide exchange Factor 1 (GBF1) domain. TGGT1_264090 contains a
225 TRAPPC11 domain. TGGT1_301410 contains both an ENTH domain and a Tepsin
226 domain. Two proteins contain functional domains that suggested they may have functions
227 related to the secretory system, but do not appear to be direct orthologs of any known
228 Golgi proteins. TGGT1_294730 contains an ancestral coatomer element 1 (ACE1) domain
229 from Sec16/Sec31 yet lacked other key domains found in these proteins. TGGT1_230400
230 contains a WIP-related protein domain but appears to only have orthologs in other
231 coccidian parasites (46). The final four selected genes (TGGT1_216370, TGGT1_207370,
232 TGGT1_258080, and TGGT1_240220) are hypothetical proteins that contained no
233 identifiable functional domains aside from predicted CC domains and had orthologs only
234 in cyst-forming coccidia.
235 To verify these candidate Golgi proteins, we endogenously tagged each protein at
236 its C-terminus with an auxin-inducible degron coupled to a 3xHA epitope tag in a TIR1

237 strain (37). We then expressed the Golgi marker GRASP55-YFP in each line and used
238 IFA to assess the localization of each gene (36). All eleven genes either colocalized with
239 GRASP55 or were closely adjacent, confirming their association with the *Toxoplasma*
240 Golgi apparatus (Fig 4). Based on their localization and functional domains, we assigned
241 names to each of the eleven proteins.
242 TGGT1_311400 was designated Sec31, TGGT1_294730 as Sec16-like protein (Sec16-
243 L), TGGT1_264090 as TRAPPC11-like protein (TRAPPC11), TGGT1_290310 as COG1,
244 TGGT1_232190 as GBF1, and TGGT1_230400 as WIP-related Protein Domain-
245 containing Protein (WPDP). The hypothetical protein TGGT1_258080 was also recently
246 identified by Marsilia et al., so we adopted their nomenclature and named it Golgi
247 Localizing Protein 1 (GLP1). The hypothetical proteins TGGT1_216370, TGGT1_207370,
248 TGGT1_240220 were designated as Golgi Localizing Protein 2, 3, and 4, respectively
249 (GLP2-4). Upon further inspection, we noticed that the extent to which each protein
250 colocalized with GRASP55 varied. Sec31, Sec16-L, and GLP3 appeared to localize
251 upstream of GRASP55 in the secretory pathway (Fig 4A, B, and H). Sec31 and Sec16 are
252 both known to localize to ER exit sites where they play roles in anterograde transport (47).
253 While GLP3 does not contain any domains that hint at its function, its similar localization
254 to Sec31 and Sec16-L suggests it may also play a role in early anterograde transport.
255 TRAPPC11, COG1, GBF1, GLP2, and WPDP all appeared to mostly colocalize with
256 GRASP55, indicating a primary localization in the cis-medial Golgi (Fig 4C-G and I).
257 TRAPPC11 and WPDP displayed some additional signal downstream of GRASP55,
258 suggesting they may also localize to the trans Golgi network (Fig 4C and G). Finally,
259 Tepsin, GLP1, and GLP4 localized downstream of GRASP55, indicating that they likely
260 are restricted to the trans Golgi network (Fig 4J and K).
261
262 **Functional analysis of novel proteins**

263 We next used the AID system to assess how depletion of each novel Golgi protein
264 would affect parasite fitness. Five of the eleven strains (Sec31, GBF1, COG1, Tepsin,
265 and TRAPPC11) were found to be completely deficient in plaque formation, indicating that
266 these proteins are essential for parasite survival (Fig 5A). Sec31 exhibited a severe growth
267 arrest, with nearly all vacuoles containing only a single parasite after 24 hours of growth
268 in the presence of IAA (Fig 5B). Despite the severe growth defect, Sec31-depleted
269 parasites appeared to have normal overall morphology as assessed by IMC6 staining.
270 GBF1 also exhibited a severe growth arrest (Fig 5C). However, in contrast to Sec31, many
271 GBF1-depleted parasites also exhibited defective IMC morphology. Both COG1 and
272 Tepsin-depleted parasites did not exhibit growth arrest at 24 hours but had severe defects
273 in morphology, such as large gashes in the cytoskeleton marked by IMC6 (Fig 5D, E). The
274 last essential protein, TRAPPC11, did not exhibit growth arrest or any apparent defects in
275 overall morphology as assessed by IMC6 staining after 24 hours of IAA treatment (Fig
276 5F).
277 The remaining six proteins were found by plaque assay to be non-essential, but
278 their depletion resulted in a statistically significant reduction in lytic ability (Fig 6A). The
279 severity of the defect varied widely among the six proteins. The most severe growth defect
280 (91.8%) was observed for GLP2. The remaining five proteins exhibited more modest
281 reductions – 25.7% for Sec16-L, 21.0% for WPDP, 14.2% for GLP1, 40.5% for GLP3,
282 37.9% for GLP4. Despite the reduction in fitness, all six of these proteins exhibited no
283 obvious defects in morphology by IFA (Fig 6B-G).
284
285 **Discussion**
286 In this study, we identified and characterized the novel Golgi protein ULP1 as a
287 critical regulator of parasite growth and used it as a probe to identify and characterize
288 additional novel Golgi proteins. Our analysis of ULP1 demonstrated that the protein

289 localizes to the cis-medial Golgi and plays an important role in parasite replication. Loss
290 of the protein by either AID-mediated knockdown or gene knockout resulted in a severe
291 defect in plaque size. Our findings contrast with that of Marsilia et al. who showed a
292 complete loss of lytic ability upon ULP1 knockdown and place its primary localization in
293 the trans-Golgi network (32). While the conditional knockdown strains may vary in the
294 phenotypes observed, the ULP1 knockout indicates that the protein is not strictly required
295 for parasite survival. ULP1 is an interesting protein because it is unique to cyst-forming
296 coccidia yet is structurally homologous to the conserved eukaryotic trafficking factor
297 p115/Uso1. Studies in mammalian cells, *Drosophila*, and yeast have demonstrated that
298 p115/Uso1 has a wide range of essential functions including tethering COPI vesicles to
299 the Golgi, transporting vesicles from the ER to the Golgi, and facilitating SNARE complex
300 assembly (48–53). Loss of p115/Uso1 has been shown to result in fragmentation of the
301 Golgi and accumulation of Golgi-derived vesicles (54). In addition to its localization to the
302 Golgi apparatus, the protein has been observed associating with the spindle poles, and
303 loss of the protein has been shown to impair mitosis (55,56). While we did not identify any
304 apparent defects in trafficking of markers to key secretory organelles or loss of Golgi
305 integrity upon ULP1 knockdown, we did observe a significant reduction in replicative ability
306 which could suggest that ULP1 plays a role in cell cycle regulation, similar to p115/Uso1.
307 P115/Uso1 is known to interact with several trafficking proteins including Rab1,
308 GBF1, COG2, GM130, and SNARE complex components Syntaxin 5, Bet1 and Bos1
309 (45,51,57–59). Our IP analysis was highly enriched for all eight COG complex subunits,
310 with COG2 being the second most enriched. Marsilia et. al also identified all eight
311 components of the COG complex in their ULP1 IP, further supporting the legitimacy of
312 these interactions (32). Interestingly, we did not identify any of the other known p115/Uso1
313 interacting proteins. While these other proteins may have been lost during processing, it
314 is also possible that ULP1 function has diverged enough from p115/Uso1 such that it does

315 not bind to these proteins and instead uses other parasite-specific proteins to fulfill these
316 roles. Supporting this, the novel Golgi protein GLP2 was found to IP with ULP1 in both
317 Marsilia et. al and our study. p115/Uso1 has been shown to bind to Cdk1 and loss of p115
318 was demonstrated to reduce Cdk1 activation (56). Interestingly, we identified a CDK-
319 related kinase, Crk2, in our IP analysis. Given that ULP1 depletion leads to a decrease in
320 replication rate, it is possible that interaction with Crk2 plays a role in *T. gondii* mitosis.
321 Alternatively, the replication defect could be due to general ER stress caused by alteration
322 of the secretory pathway (60). When comparing the remaining results of our IP with
323 Marsilia et. al, several differences are observed. They identified a wide variety of other
324 proteins including eight SNARE proteins, four AP-5 complex proteins, and five COPI
325 complex subunits that were either absent from our analysis or did not reach the two-fold
326 enrichment cut-off. Additionally, the authors noted that over 20 IMC proteins and Rab11b,
327 which is critical for IMC biogenesis, were enriched in their ULP1 IP. However, we did not
328 observe enrichment for any of these proteins. Similarly, our IP identified Crk2, Rab7,
329 Vps35, TgEpsL, AP1-γ, and a Sec23/Sec24 trunk domain-containing protein while the
330 other study did not. These disparities likely arise from differences in sample processing,
331 and further analysis of ULP1 binding partners will be needed to create a more definitive
332 picture of the ULP1 interactome.

333 Using ULP1 as bait in both TurboID and IP experiments, we were able to identify
334 11 previously uncharacterized Golgi-associated proteins. Sec31, COG1, GBF1, Tepsin,
335 and TRAPPC11 were found to be essential, which is unsurprising due to their critical
336 conserved functions in other eukaryotes. Two of these proteins, Sec31 and GBF1, caused
337 an immediate growth arrest upon depletion, likely due to a block in the secretory pathway
338 that prevents the continuation of the cell cycle. Sec31 acts as a component of the COPII
339 complex, which facilitates anterograde transport from the ER to the Golgi and causes
340 growth arrest when depleted in *Trypanosomes* (47,61,62). We observed the *T. gondii*

341 Sec31 localizing upstream of GRASP55 in the secretory pathway, indicating that it likely
342 localizes to ER exit sites as in other eukaryotes. The localization of this protein to this
343 subcompartment of the Golgi represents a valuable new marker for this region of the
344 secretory pathway in *T. gondii*. GBF1 is a Golgi-resident guanine nucleotide exchange
345 factor that regulates COPI vesicle-mediated transport by activating ADP-ribosylation
346 factor (Arf) proteins (63,64). We observed *Toxoplasma* GBF1 localizing to the cis-medial
347 Golgi, which agrees with its function in other systems.

348 Unlike Sec31 and GBF1, the remaining three essential proteins, COG1, Tepsin,
349 and TRAPPC11, did not exhibit an immediate growth arrest upon depletion. COG1 is a
350 component of the COG complex, which acts in the retrograde transport pathway by
351 tethering COPI-coated vesicles that are used for recycling Golgi-resident enzymes such
352 as glycosyltransferases back to the Golgi (65,66). Several *T. gondii* proteins such as
353 GAP50 and CST1 have been shown to be glycosylated, and this modification is required
354 for their proper targeting and function (67,68). In agreement with this, Marsilia et. al
355 demonstrated that O-glycosylation is disrupted upon COG3 or COG7 depletion (32). This
356 function is primarily carried out in the cis/medial Golgi, which matches our observed
357 colocalization of COG1 with GRASP55. Tepsin is an accessory protein that associates
358 with the AP-4 complex, which plays a role in vesicular trafficking of proteins at the trans-
359 Golgi network (69,70). Knockdown of either COG1 or Tepsin resulted in severe defects in
360 IMC morphology, suggesting that loss of either protein causes issues with the secretory
361 pathway ultimately leading to defects in IMC biogenesis. TRAPPC11, on the other hand,
362 did not exhibit any obvious morphological defects. TRAPPC11 was observed colocalizing
363 with GRASP55 in the cis-medial Golgi. Since TRAPPC11 functions in anterograde vesicle
364 transport as a member of the TRAPPIII tethering complex, it is possible that *Toxoplasma*
365 TRAPPC11 could play a key role in trafficking of effector proteins like ROPs and MICs,

366 leading to a defect in invasion and/or egress (71). Further studies will be needed to assess
367 precisely how each of these essential proteins affects parasite fitness.

368 Two of the identified proteins, Sec16-L and WPDP, do not appear to be direct
369 orthologs of known Golgi proteins but contain domains that suggested conserved
370 functions. Sec16-L contains the ACE1 domain from Sec16, an essential COPII vesicle
371 coat protein required for ER transport vesicle budding and formation of ER exit sites (72).
372 However, it is missing the Sec16 conserved C-terminal domain which facilitates binding
373 to Sec23 and is essential for function (73). Sec16-L's localization upstream of GRASP55
374 further supports its functional similarity to Sec16 and provides another marker of this early
375 subcompartment of the secretory pathway in addition to Sec31. While Sec16 is essential
376 in other systems, Sec16-L had a relatively modest fitness defect upon conditional
377 knockdown and its ortholog in *P. falciparum* (PF3D7_1119900) is also predicted to be
378 dispensable (74). It is possible that another protein has adopted this function in *T. gondii*
379 and other apicomplexans, rendering this protein redundant. WPDP contains a WIP-related
380 protein domain which is known to facilitate actin binding. Numerous Golgi-resident actin-
381 binding proteins have previously been identified in mammalian cells and the actin
382 cytoskeleton has been shown to be critical for maintaining Golgi structure and facilitating
383 vesicular trafficking (75). Similar to Sec16-L, WPDP had a modest phenotype upon
384 conditional knockdown. It is possible that WPDP may be one of several actin-binding
385 proteins that help maintain Golgi structure in *T. gondii* and related apicomplexans.

386 We additionally identified four novel parasite-specific Golgi proteins, GLP1-4,
387 which were all found to be non-essential. GLP3, which we identified as an interactor of
388 ULP1 by IP, was found to localize upstream of GRASP55 like Sec16-L and Sec31, and
389 therefore could play a role in ER to Golgi vesicle transport. GLP1 and GLP4 both localize
390 downstream of GRASP55, suggesting they function in the trans-Golgi network. Both
391 proteins exhibit only a relatively small reduction in plaque size upon their depletion.

392 Interestingly, the two proteins are similar in size and both contain a region with one larger
393 coiled-coil domain closely followed by two shorter coiled-coil domains. While their
394 sequence similarity does not suggest they are paralogs, their similar localizations,
395 phenotypes, and structural compositions could indicate possible functional redundancy.
396 Finally, GLP2 was found to localize to the cis-medial Golgi and caused a dramatic 91.8%
397 reduction in plaque size when depleted. Despite this, we did not observe any obvious
398 growth defects or morphological changes by IFA, suggesting that loss of GLP2 may affect
399 either invasion or egress rather than replication. Interestingly, all of the GLPs contain
400 several predicted coiled-coil domains and are only found in the cyst-forming coccidia.
401 Coiled-coil domain-containing proteins such as the golgin proteins GM130, giantin, and
402 CASP are known to act as tethering factors in other eukaryotes (76). As the GLPs are
403 unique to the cyst-forming coccidia, it is possible they could use their CC domains to act
404 as Golgi tethering factors that carry out unique functions in this subset of apicomplexan
405 parasites.

406 Together, this study reveals a total of 12 novel Golgi-associated proteins including
407 several that are essential and others that are parasite-specific. Their identification provides
408 valuable new markers for the secretory pathway and provides exciting candidates for
409 further functional analysis. Due to the apicomplexan-specific nature of several of these
410 proteins, they represent both novel cell biology and potential targets for therapeutic
411 intervention.

412

413

414 **Materials and Methods**

415

416 ***T. gondii* and host cell culture**

417 Parental *T. gondii* RHΔ*hxgprtΔku80* (wild-type) and subsequent strains were
418 grown on confluent monolayers of human foreskin fibroblasts (BJ, ATCC, Manassas, VA)
419 at 37°C and 5% CO_2 in Dulbecco's Modified Eagle Medium (DMEM) supplemented with
420 5% fetal bovine serum (Gibco), 5% Cosmic calf serum (Hyclone), and 1x penicillin-
421 streptomycin-L-glutamine (Gibco). Constructs containing selectable markers were
422 selected using 1 μM pyrimethamine (dihydrofolate reductase-thymidylate synthase
423 [DHFR-TS]), 50 μg/mL mycophenolic acid-xanthine (HXGPRT), or 40 μM chloramphenicol
424 (CAT) (77–79). For AID conditional knockdown experiments, media was supplemented
425 with 500 μM indoleacetic acid (Sigma-Aldrich; I2886) or vehicle control.

426

427 **Antibodies**

428 The HA epitope was detected with mouse monoclonal antibody (mAb) HA.11
429 (BioLegend; 901515). The V5 epitope was detected with mouse mAb anti-V5 (Invitrogen;
430 R96025). *Toxoplasma*-specific antibodies include rabbit pAb anti-IMC6 (80), rat pAb anti-
431 DrpB (23), guinea pig pAb anti-NHE3 (81), mouse pAb anti-SERCA (82), mouse mAb anti-
432 ROP7 (1B10) (83), mouse mAb anti-MIC2 (6D10) (84), mouse pAb anti-GRA14 (83),
433 mouse mAb anti-ATrx1 (11G8) (85), mouse mAb anti-F1β subunit (5F4) (86), and mouse
434 pAb anti-ROP13 (87).

435

436 **Endogenous epitope tagging and knockout**

437 For C-terminal endogenous tagging, a pU6-Universal plasmid containing a
438 protospacer against the 3′ untranslated region (UTR) of the target protein approximately
439 100 bp downstream of the stop codon was generated, as described previously (34). A

440 homology-directed repair (HDR) template was PCR amplified using the Δ*ku80*-dependent
441 LIC vector pmAID3xHA.LIC-HPT, pmIAA73xHA.LIC-HPT, p3xHA.LIC-DHFR, p3xV5.LIC-
442 DHFR, or pTurboID3xHA.LIC-DHFR, all of which include the epitope tag, 3′ UTR, and a
443 selection cassette (88). The 60-bp primers include 40 bp of homology immediately
444 upstream of the stop codon or 40 bp of homology within the 3′ UTR downstream of the
445 CRISPR/Cas9 cut site. For knockout of ULP1, the protospacer was designed to target the
446 coding region of ULP1, ligated into the pU6-Universal plasmid and prepared similarly to
447 the endogenous tagging constructs. The HDR template was PCR amplified from a pJET
448 vector containing the HXGPRT drug marker driven by the NcGRA7 promoter using
449 primers that included 40 bp of homology immediately upstream of the start codon or 40
450 bp of homology downstream of the region used for homologous recombination for
451 endogenous tagging. All primers that were used for pU6-Universal plasmids and HDR
452 templates are listed in Table S3.
453 For all tagging and knockout constructs, approximately 50 µg of the sequence-
454 verified pU6-Universal plasmid was precipitated in ethanol, and the PCR-amplified HDR
455 template was purified by phenol chloroform extraction and precipitated in ethanol. Both
456 constructs were electroporated into the appropriate parasite strain. Transfected cells were
457 allowed to invade a confluent monolayer of HFFs overnight, and appropriate selection was
458 subsequently applied. Successful tagging was confirmed by IFA, and clonal lines of
459 tagged parasites were obtained through limiting dilution.
460
461 **Immunofluorescence assay**
462 Confluent HFF cells were grown on glass coverslips and infected with *T. gondii*.
463 After 24 hours, the coverslips were fixed with 3.7% formaldehyde in PBS and processed
464 for immunofluorescence as described (87). Primary antibodies were detected by species-
465 specific secondary antibodies conjugated to Alexa Fluor 594/488 (ThermoFisher).

466 Coverslips were mounted in Vectashield (Vector Labs), viewed with an Axio Imager.Z1
467 fluorescent microscope and processed with ZEN 2.3 software (Zeiss).
468
469 **Western blot**
470 Parasites were lysed in 1x Laemmli sample buffer with 100 mM DTT and boiled at
471 100°C for 5 minutes. Lysates were resolved by SDS-PAGE and transferred to
472 nitrocellulose membranes, and proteins were detected with the appropriate primary
473 antibody and corresponding secondary antibody conjugated to horseradish peroxidase.
474 Chemiluminescence was induced using the SuperSignal West Pico substrate (Pierce) and
475 imaged on a ChemiDoc XRS+ (Bio-Rad).
476
477 **Plaque assay**
478 HFF monolayers were infected with 200 parasites per well of individual strains (-/+
479 IAA for AID strains) and allowed to form plaques for 7 days. Cells were then fixed with ice-
480 cold methanol and stained with crystal violet. To quantify plaque size, the areas of 50
481 plaques per condition were measured using ZEN software (Zeiss). To quantify plaque
482 number, the total number of plaques in each condition was counted manually. All plaque
483 assays were performed in triplicate. Graphical and statistical analyses were performed
484 using Prism GraphPad 8.0.
485
486 **Quantification of parasites per vacuole**
487 Parasites were pre-treated with IAA or vehicle control for 18 hours prior to infecting
488 coverslips. After coverslips were infected, parasites were allowed to grow -/+ IAA for 30
489 hours prior to fixation and staining with mouse anti-HA (detecting $ULP1^{AID}$) and rabbit anti-
490 IMC6. For each condition, the number of parasites per vacuole (1, 2, 4, 8, 16, or ≥32) was

491 counted for >100 vacuoles across 10 different fields. Experiments were performed in
492 triplicate. Significance was determined using multiple two-tailed t tests.
493
494 **Affinity capture of biotinylated proteins**
495 For affinity capture of proteins from whole cell lysates, HFF monolayers infected
496 with ULP1^{TurboID} or control parasites (RHΔ*hxgprt*Δ*ku80*, WT) were grown in medium
497 containing 150 μM biotin for 30 hours. Intracellular parasites in large vacuoles were
498 collected by manual scraping, washed in PBS, and lysed in radioimmunoprecipitation
499 assay (RIPA) buffer (50 mM Tris [pH 7.5], 150 mM NaCl, 0.1% SDS, 0.5% sodium
500 deoxycholate, 1% NP-40) supplemented with Complete Protease Inhibitor Cocktail
501 (Roche) for 30 min on ice. Lysates were centrifuged for 15 min at 14,000 x g to pellet
502 insoluble material, and the supernatant was incubated with Streptavidin Plus UltraLink
503 resin (Pierce) overnight at 4°C under gentle agitation. Beads were collected and washed
504 five times in RIPA buffer, followed by three washes in 8 M urea buffer (50 mM Tris-HCl
505 [pH 7.4], 150 mM NaCl) (89). Samples were submitted for on-bead digests and
506 subsequently analyzed by mass spectrometry. The experiment was performed in
507 duplicate.
508
509 **Immunoprecipitation assay**
510 ULP1^{3XHA} was isolated from 5×10^9 *T. gondii* RH tachyzoites lysed in NP-40 lysis
511 buffer (1% NP-40, 150 mM NaCl, 50 mM Tris [pH 8.0]) supplemented with complete
512 protease inhibitor (Roche). The insoluble material was removed from the lysate by
513 centrifugation at 10,000 x *g* for 20 minutes. The soluble lysate fraction was incubated with
514 rat anti-HA affinity matrix (Roche) for 3 hours at room temperature with gentle agitation.
515 After washing in NP-40 lysis buffer, the bound protein was eluted using high pH (100 mM
516 triethylamine, pH 11.5), dried to a pellet, and submitted for mass spectrometry.

517

518 **Mass spectrometry**

519 Samples were resuspended in digestion buffer (8M Urea, 0.1M Tris-HCl [pH 8.5]) and then
520 were reduced, alkylated, and digested by sequential addition of Lys-C and trypsin
521 proteases. Samples were then desalted using C18 tips (Pierce) and fractionated online
522 using a 75-µm inner-diameter fritted fused silica capillary column with a 5-µm pulled
523 electrospray tip and packed in-house with 25 cm of C18 (Dr. Maisch GmbH) 1.9-µm
524 reversed-phase particles. The gradient was delivered by a 140-minute gradient of
525 increasing acetonitrile and eluted directly into a Thermo Orbitrap Fusion Lumos instrument
526 where MS/MS spectra were acquired by Data Dependent Acquisition (DDA). Data analysis
527 was performed using ProLuCID and DTASelect2 implemented in Integrated Proteomics
528 Pipeline IP2 (Integrated Proteomics Applications) (90–92). Database searching was
529 performed using a FASTA protein database containing *T. gondii* GT1-translated open
530 reading frames downloaded from ToxoDB. Protein and peptide identifications were filtered
531 using DTASelect and required a minimum of two unique peptides per protein and a
532 peptide-level false positive rate of less than 5% as estimated by a decoy database
533 strategy. Candidates were ranked by spectral count comparing experimental versus
534 control samples (93). TurboID results were filtered to include only proteins that were at
535 least two-fold enriched with a difference of >5 spectral counts when comparing ULP1^{TurboID}
536 samples versus control samples. IP results were filtered to include only proteins that were
537 at least two-fold enriched when comparing ULP1^{3xHA} IP samples versus control samples.

538

539 **Bioinformatic analysis of novel proteins**

540 Functional domains were identified using a combination of Phyre2, Interpro
541 Domains, PFAM, and Panther analysis (28,30,94,95). Coiled coil domains were predicted

542 using DeepCoil2 using a probability cut-off of 0.5 (31). Orthology was determined using
543 OrthoMCL and BLASTp search against the VEuPathDB database (46).
544
545 **Acknowledgements**
546 We thank Vern Carruthers for supplying the anti-MIC2 antibody, Gustavo Arrizabalaga for
547 supplying the anti-NHE3 antibody, and David Sibley for supplying the anti-SERCA
548 antibody. This work was supported by NIH grants AI123360 to P.J.B, and GM089778 to
549 J.A.W. R.R.P. and V.Y. were supported by the Ruth L. Kirschstein National Research
550 Service Award AI007323. R.R.P was additionally supported by the Ruth L. Kirschstein
551 National Research Service Award GM007185 and the UCLA Molecular Biology Institute
552 Whitcome Fellowship. J.J.Q was supported by a Milton Gottlieb endowment award and by
553 a Beckman Scholars Award through the Arnold and Mabel Beckman Foundation.
554
555 **Competing Interests**
556 The authors declare no competing interests.
557
558

Figure 1

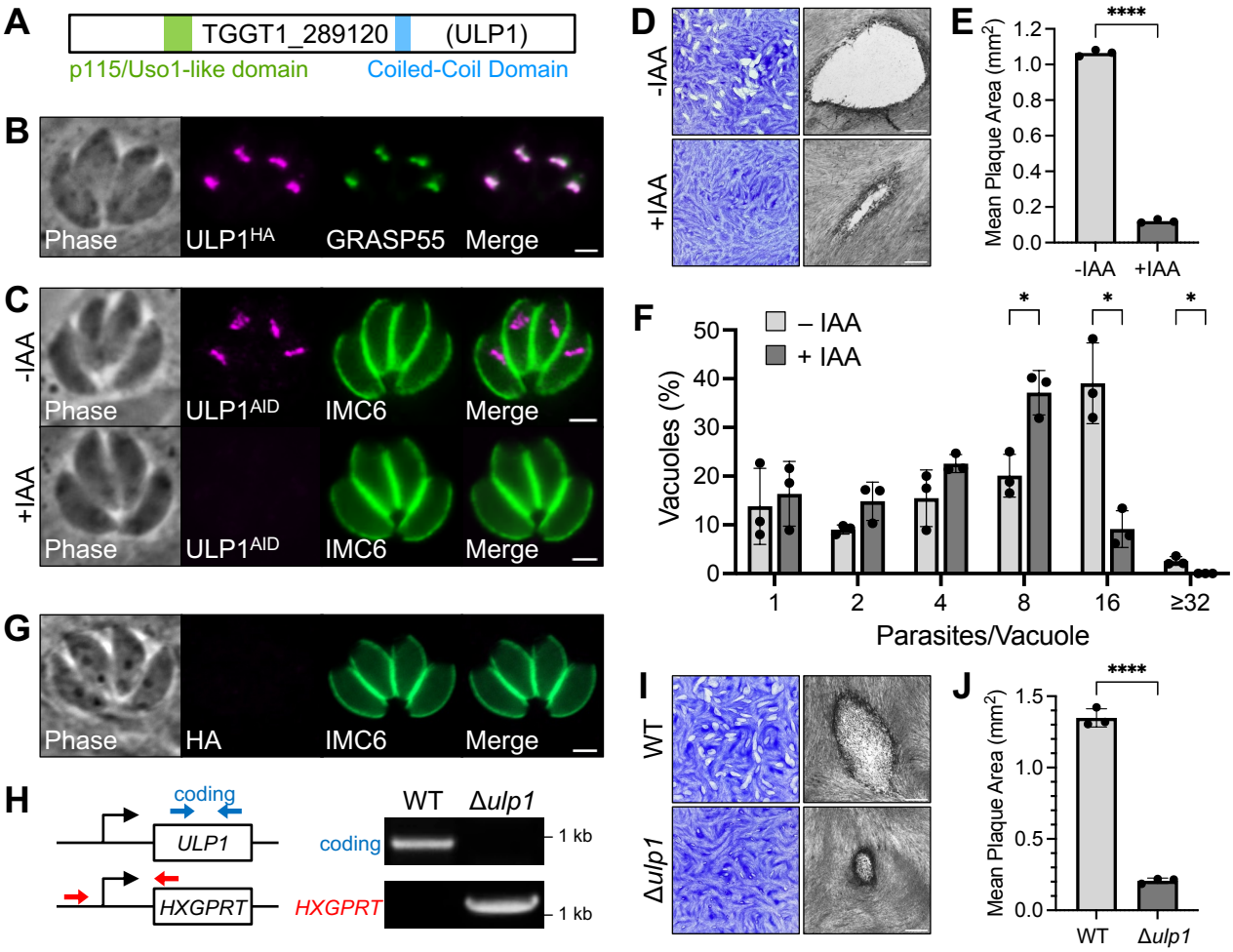
A
TGGT1_289120
(ULP1)
p115/Uso1-like domain
Coiled-Coil Domain
B
Phase
ULP1HA
GRASP55
Merge
C
-IAA
+IAA
Phase
ULP1AID
IMC6
Merge
G
Phase
HA
IMC6
Merge
H
coding
ULP1
HXGPRT
WT
Δulp1
coding
HXGPRT
1 kb
1 kb
D
-IAA
+IAA
E
Mean Plaque Area (mm2)
****
-IAA
+IAA
F
– IAA
+ IAA
Vacuoles (%)
Parasites/Vacuole
1
2
4
8
16
≥32
I
WT
Δulp1
J
Mean Plaque Area (mm2)
****
WT
Δulp1

559 **Fig 1. ULP1 is a novel Golgi-localizing protein that is important for parasite fitness.**
560 A) Gene model of TGGT1_289120 (ULP1) showing its p115/Uso1-like domain and
561 predicted CC domain. B) IFA showing that ULP1 colocalizes with the Golgi apparatus
562 marker GRASP55-YFP. Magenta = anti-HA detecting ULP1^{3xHA}, Green = GRASP55-YFP.
563 C) IFA showing that ULP1^{AID} localizes normally and is depleted after 24 hours of IAA
564 treatment. Magenta = anti-HA detecting ULP1^{AID}, Green = anti-IMC6. D) Plaque assay for
565 ULP1^{AID} parasites -/+IAA shows that depletion of ULP1 results in a severe reduction in
566 overall lytic ability. E) Quantification of plaque size for plaque assays shown in panel D.
567 Significance was determined using two-tailed t test. **** = $P < 0.0001$. F) Quantification of
568 the number of parasites per vacuole for ULP1^{AID} parasites treated with IAA or vehicle
569 control after 24 hours of growth. Significance was determined using multiple two-tailed t
570 tests. * = $P < 0.05$. G) IFA of Δ*ulp1* parasites confirms loss of ULP1^{3xHA} signal. Magenta =
571 anti-HA, Green = anti-IMC6. H) PCR verification for genomic DNA of WT and Δ*ulp1*
572 parasites. Diagram indicates the binding location of primers used to amplify the ULP1
573 coding sequencing (blue arrows) and the site of recombination for the knockout (red
574 arrows). I) Plaque assays of WT and Δ*ulp1* parasites. J) Quantification of plaque size for
575 plaque assays shown in panel I. Statistical significance was determined using a two-tailed
576 t test. **** = $P < 0.0001$. Scale bars for plaque assays = 0.5 mm. Scale bars for IFAs = 2
577 µm.
578
579

Figure 2

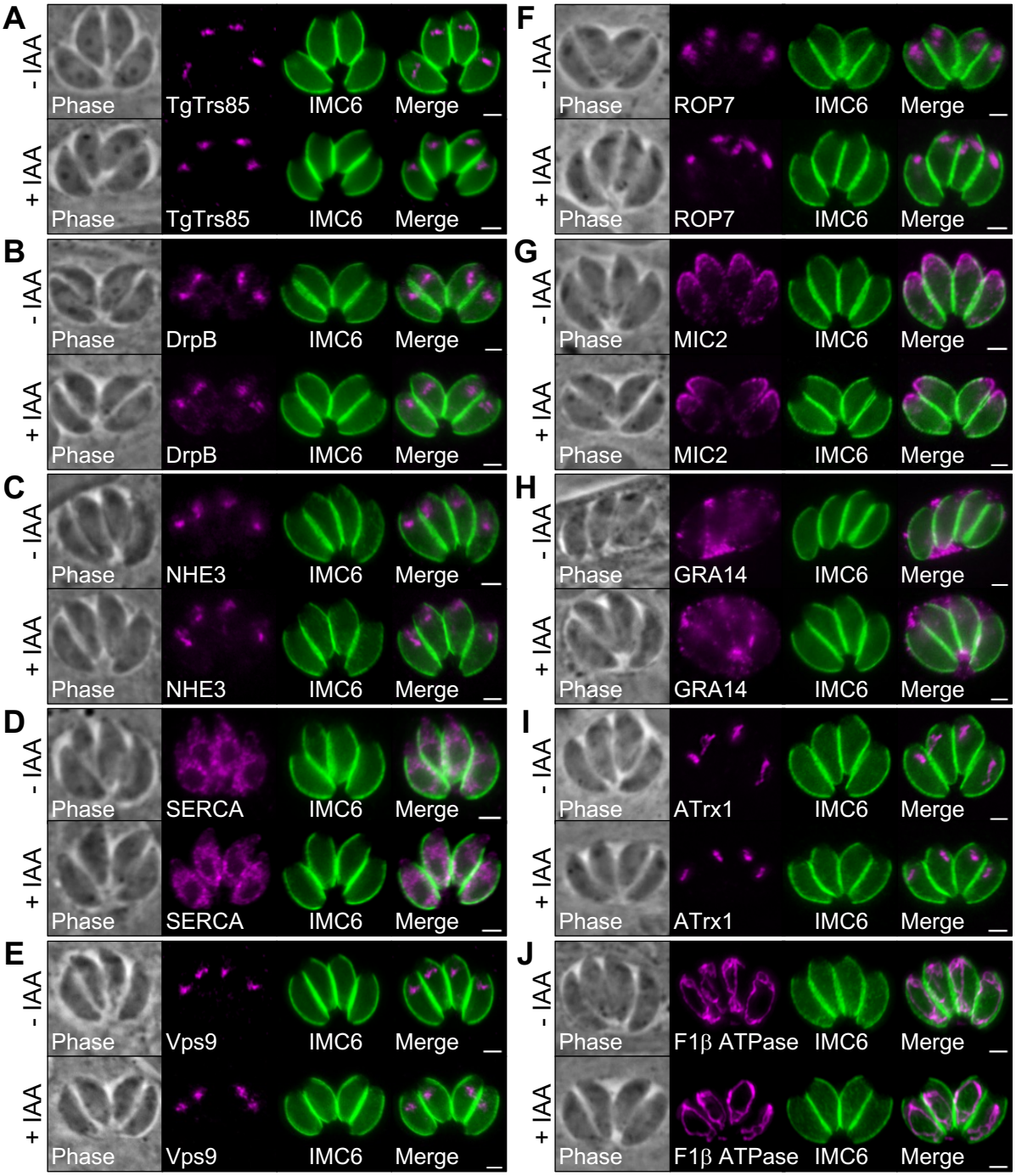
A
- IAA
+ IAA
Phase
TgTrs85
IMC6
Merge
B
DrpB
C
NHE3
D
SERCA
E
Vps9
F
ROP7
G
MIC2
H
GRA14
I
ATrx1
J
F1β ATPase

580 **Fig 2. Depletion of ULP1 does not affect overall organellar morphology.** IFAs
581 comparing the overall morphology of various *T. gondii* organelles in control vs. ULP1-
582 depleted parasites. A) Golgi apparatus morphology is unaffected by depletion of ULP1.
583 Magenta = anti-V5 detecting TgTrs85^{3xV5}, Green = anti-IMC6. B) Post-Golgi vesicle
584 morphology is unaffected by depletion of ULP1. Magenta = anti-DrpB, Green = anti-IMC6.
585 C) PLVAC morphology is unaffected by depletion of ULP1. Magenta = anti-NHE3, Green
586 = anti-IMC6. D) ER morphology is unaffected by depletion of ULP1. Magenta = anti-
587 SERCA, Green = anti-IMC6. E) ELC morphology is unaffected by depletion of ULP1.
588 Magenta = anti-V5 detecting Vps9^{3xV5}, Green = anti-IMC6. F) Rhoptry morphology is
589 unaffected by depletion of ULP1. Magenta = anti-ROP7, Green = anti-IMC6. G)
590 Microneme morphology is unaffected by depletion of ULP1. Magenta = anti-MIC2, Green
591 = anti-IMC6. H) Dense granule morphology is unaffected by depletion of ULP1. Magenta
592 = anti-GRA12, Green = anti-IMC6. I) Apicoplast morphology is unaffected by depletion of
593 ULP1. Magenta = anti-ATrx1, Green = anti-IMC6. J) Mitochondrion morphology is
594 unaffected by depletion of ULP1. Magenta = anti-F1β ATPase, Green = anti-IMC6. Scale
595 bars = 2 μm.
596
597

Figure 3

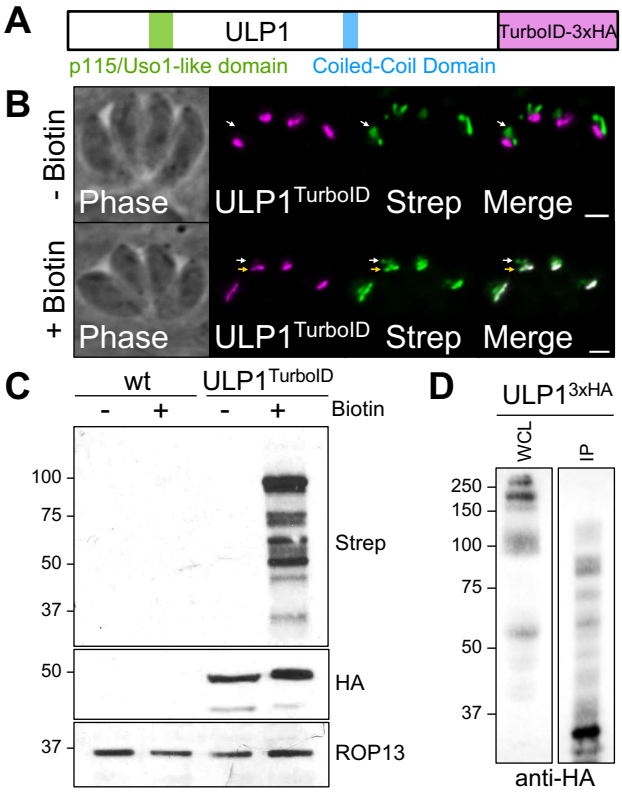
A
ULP1
TurboID-3xHA
p115/Uso1-like domain
Coiled-Coil Domain
B
- Biotin
+ Biotin
Phase
ULP1TurboID
Strep
Merge
C
wt
ULP1TurboID
- + - +
Biotin
100
75
50
37
Strep
50
HA
37
ROP13
D
ULP1 3xHA
WCL
IP
250
150
100
75
50
37
anti-HA

598 **Fig 3. Validation of ULP1 TurboID and IP.** A) The TurboID biotin ligase and a 3xHA tag
599 were fused to the C-terminus of ULP1 to generate the ULP1^{TurboID} line. B) IFA showing that
600 ULP1^{TurboID} localizes as expected and results in biotinylation of proximal proteins in a
601 biotin-dependent manner (yellow arrow). The apicoplast, which contains endogenously
602 biotinylated proteins, is denoted by white arrow. Magenta = anti-HA detecting ULP1^{TurboID},
603 Green = streptavidin. Scale bar = 2 μm. C) Western blot showing biotin-dependent
604 biotinylation of proteins in the ULP1^{TurboID} line, which is absent from a wild-type control.
605 ROP13 is used as a loading control. D) Western blot showing enrichment of ULP1^{3xHA}
606 after immunoprecipitation with anti-HA resin despite significant protein breakdown. WCL
607 = whole-cell lysate prior to IP. IP = final sample eluted from anti-HA resin.
608
609

Figure 4

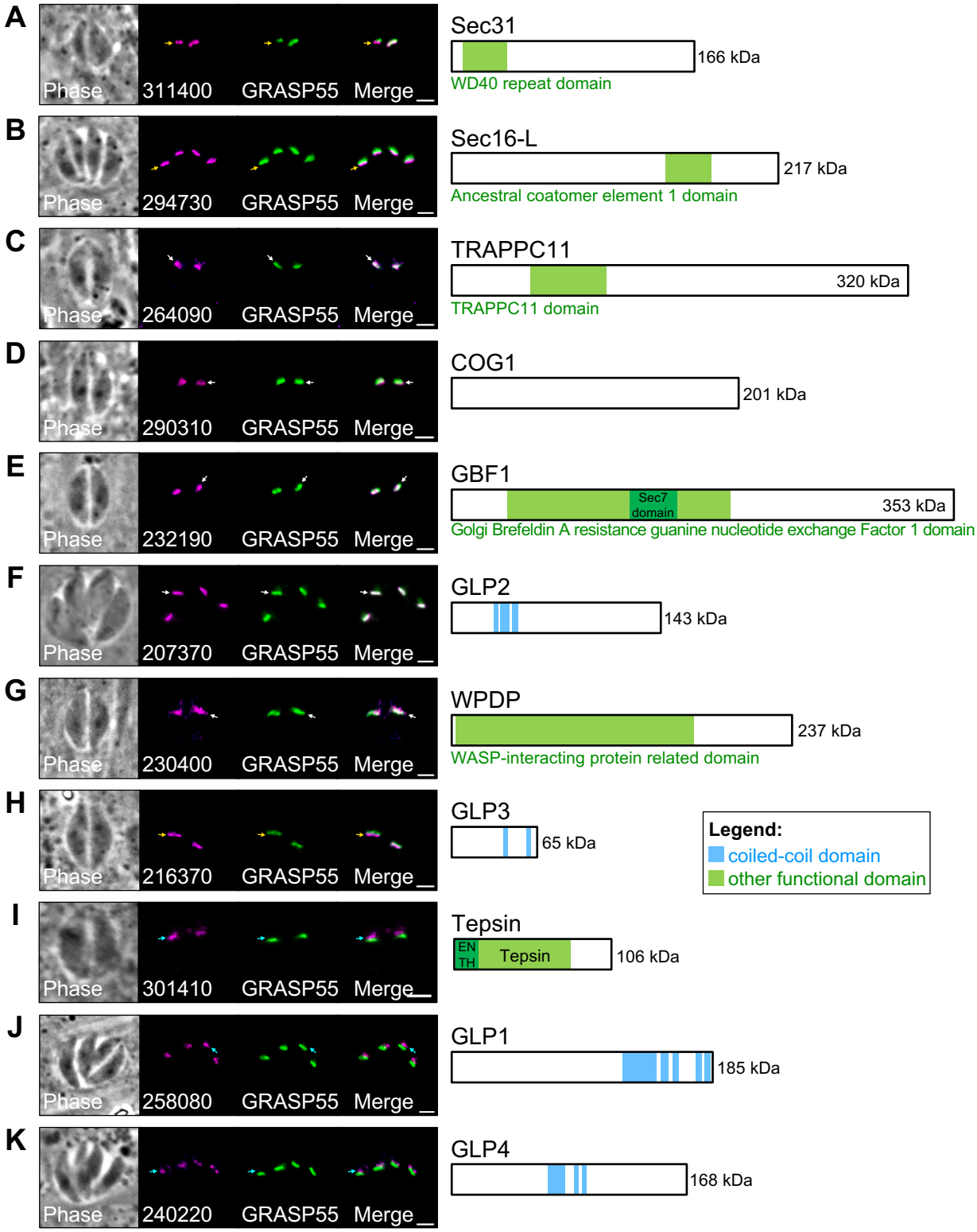
A
Phase
311400
GRASP55
Merge
Sec31
166 kDa
WD40 repeat domain
B
Phase
294730
GRASP55
Merge
Sec16-L
217 kDa
Ancestral coatomer element 1 domain
C
Phase
264090
GRASP55
Merge
TRAPPC11
320 kDa
TRAPPC11 domain
D
Phase
290310
GRASP55
Merge
COG1
201 kDa
E
Phase
232190
GRASP55
Merge
GBF1
Sec7 domain
353 kDa
Golgi Brefeldin A resistance guanine nucleotide exchange Factor 1 domain
F
Phase
207370
GRASP55
Merge
GLP2
143 kDa
G
Phase
230400
GRASP55
Merge
WPDP
237 kDa
WASP-interacting protein related domain
H
Phase
216370
GRASP55
Merge
GLP3
65 kDa
Legend:
coiled-coil domain
other functional domain
I
Phase
301410
GRASP55
Merge
Tepsin
EN TH
Tepsin
106 kDa
J
Phase
258080
GRASP55
Merge
GLP1
185 kDa
K
Phase
240220
GRASP55
Merge
GLP4
168 kDa

610 **Fig 4. ULP1 TurboID and IP hits reveals novel Golgi-associated proteins.** IFAs and
611 corresponding gene models for 11 genes identified as candidate Golgi proteins in the
612 ULP1 TurboID and IP experiments. Each gene was endogenously tagged with mAID-
613 3xHA or mIAA7-3xHA auxin-inducible degrons. White arrows indicate that the protein
614 primarily colocalizes with GRASP55-YFP. Yellow arrows indicate that the protein primarily
615 localizes upstream of GRASP55-YFP. Cyan arrows indicate that the protein primarily
616 localizes downstream of GRASP55-YFP. A) TGGT1_311400 (Sec31) localizes upstream
617 of GRASP55 and contains a WD40 repeat domain. B) TGGT1_294730 (Sec16-L)
618 localizes upstream of GRASP55 and contains an ACE1 domain. C) TGGT1_264090
619 (TRAPPC11) colocalizes with GRASP55 and contains a TRAPPC11 domain. D)
620 TGGT1_290310 (COG1) colocalizes with GRASP55 and contains no identifiable
621 functional domains. E) TGGT1_232190 (GBF1) colocalizes with GRASP55 and contains
622 a GBF1 domain. F) TGGT1_207370 (GLP2) colocalizes with GRASP55 and contains
623 three predicted CC domains within residues 273-301, 313-373, and 382-423. G)
624 TGGT1_230400 (WPDP) colocalizes with GRASP55 and contains a large WASP-
625 interacting protein related domain. H) TGGT1_216370 (GLP3) localizes downstream of
626 GRASP55 and contains two predicted CC domains within residues 337-370 and 494-527.
627 I) TGGT1_ 301410 (Tepsin) localizes downstream of GRASP55 and contains ENTH and
628 Tepsin domains. J) TGGT1_258080 (GLP1) localizes downstream of GRASP55 and
629 contains five predicted CC domains within residues 1117-1332, 1362-1407, 1425-1464,
630 1603-1646, and 1659-1701. K) TGGT1_240220 (GLP4) localizes downstream of
631 GRASP55 and contains three predicted CC domains within residues 634-747, 797-830,
632 and 850-881. Magenta = anti-HA detecting degron-tagged proteins, Green = GRASP55-
633 YFP. Scale bars = 2 μm.
634

Figure 5

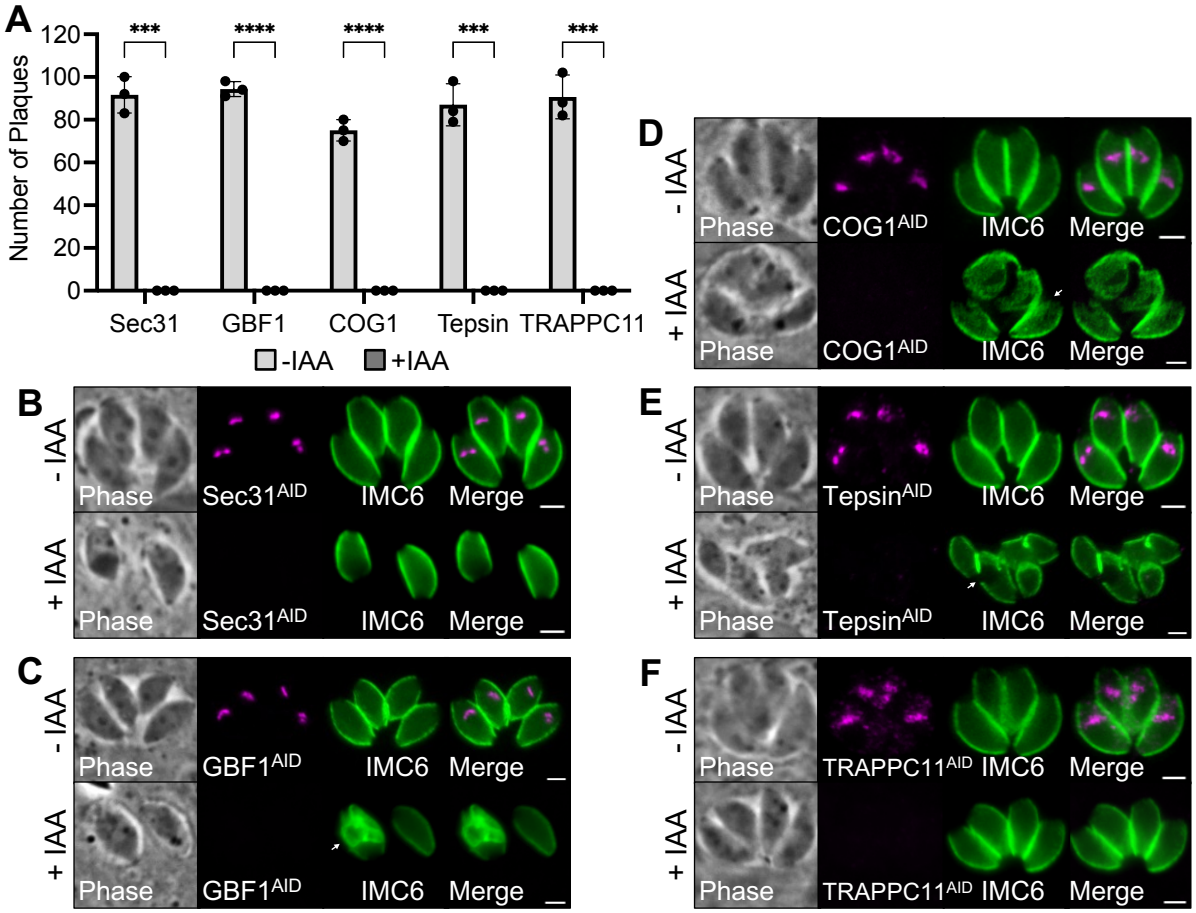
A
Number of Plaques
120
100
80
60
40
20
0
***
****
****
***
***
Sec31
GBF1
COG1
Tepsin
TRAPPC11
-IAA
+IAA
B
- IAA
+ IAA
Phase
Sec31AID
IMC6
Merge
C
GBF1AID
D
COG1AID
E
TepsinAID
F
TRAPPC11AID

635 **Fig 5. Conditional knockdown of Sec31, GBF1, COG1, Tepsin, and TRAPPC11.** A)
636 Plaque assays were performed -/+ IAA to assess how depletion of Sec31, GBF1, COG1,
637 Tepsin, or TRAPPC11 affects overall lytic ability over the course of seven days. Number
638 of plaques was quantified for each condition. Statistical significance was determined using
639 multiple two-tailed t tests (**** = $P < 0.0001$, *** = $P < 0.001$) B, C) Depletion of Sec31 or
640 GBF1 results in growth arrest. Depletion of GBF1 additionally leads to morphological
641 defects in some parasites (white arrow). C, D) Depletion of COG1 or Tepsin results in
642 morphological defects (white arrows). F) Depletion of TRAPPC11 does not result in any
643 obvious defects in morphology. Magenta = anti-HA detecting degron-tagged proteins,
644 Green = anti-IMC6. Scale bars = 2 μm.
645
646

Figure 6

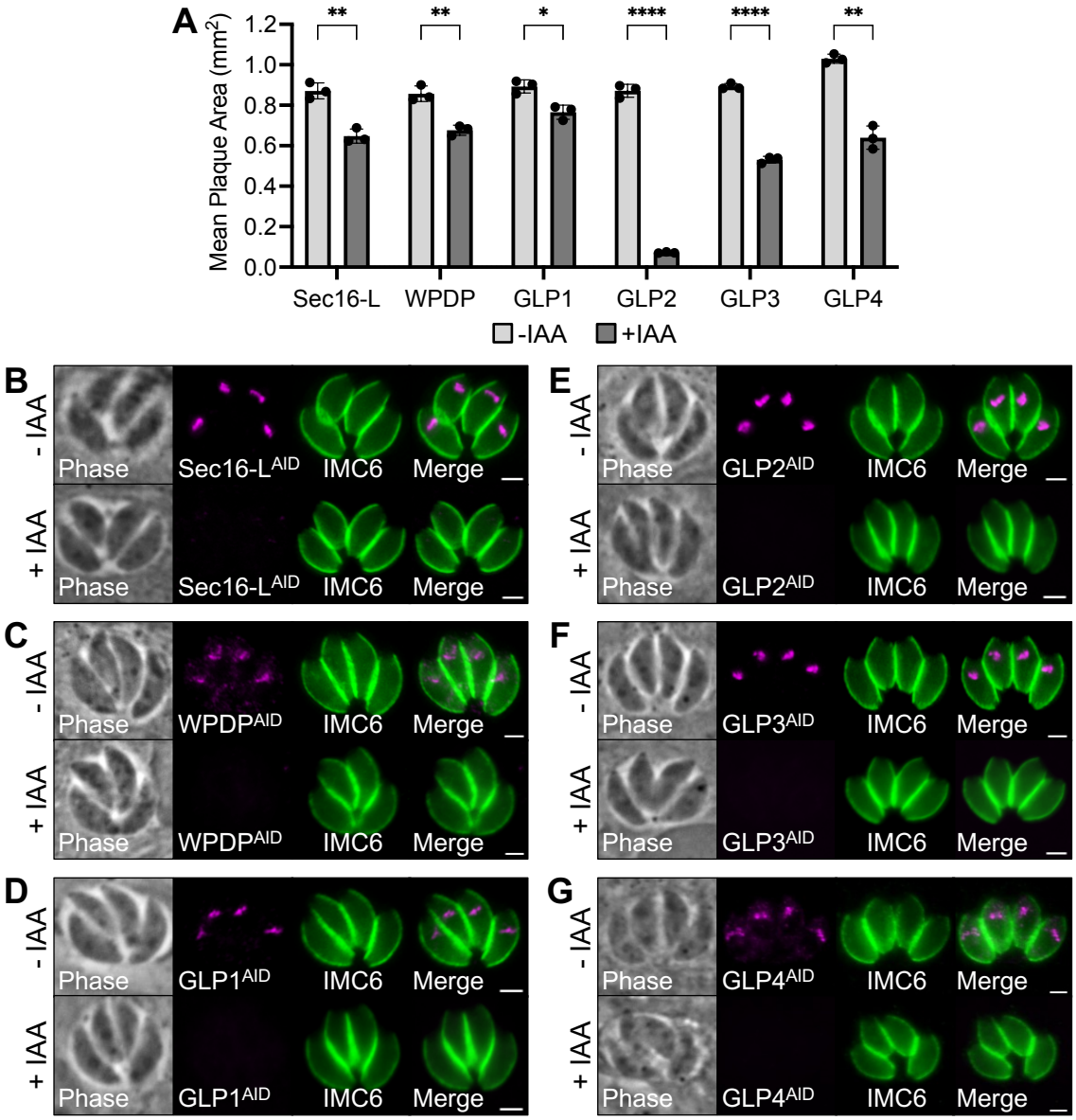
A
Mean Plaque Area (mm²)
1.2
1.0
0.8
0.6
0.4
0.2
0.0
**
**
*
****
****
**
Sec16-L
WPDP
GLP1
GLP2
GLP3
GLP4
-IAA
+IAA
B
C
D
E
F
G
- IAA
+ IAA
Phase
Sec16-L^AID
WPDP^AID
GLP1^AID
GLP2^AID
GLP3^AID
GLP4^AID
IMC6
Merge

647 **Fig 6. Conditional knockdown of Sec16-L, WPDP, GLP1, GLP2, GLP3, and GLP4.**
648 A) Plaque assays were performed -/+IAA to assess how depletion of Sec16-L, WPDP,
649 GLP1, GLP2, GLP3, and GLP4 affects overall lytic ability over the course of seven days.
650 Mean plaque area was quantified for each condition. Statistical significance was
651 determined using multiple two-tailed t tests (**** = $P < 0.0001$, *** = $P < 0.001$, ** = $P <$
652 0.01, * = $P < 0.05$.) B-G) Depletion of Sec16-L, WPDP, GLP1, GLP2, GLP3, or GLP4 does
653 not result in any obvious defects in morphology. Magenta = anti-HA detecting degron-
654 tagged proteins, Green = anti-IMC6. Scale bars = 2 μm.
655
656

Table 1

Gene ID	Abbrv.	Protein Name	TurboID		IP		ToxoDB Annotation	GWCS
			Ctrl	Exp	Ctrl	Exp		
TGGT1_289120	ULP1	Uso1-Like Protein 1	1.5	341	0	382	hypothetical protein	-3.8
TGGT1_311400	Sec31	Secretory 31	28	698.5	0	0	WD domain, G-beta repeat-containing protein	-5.53
TGGT1_294730	Sec16-L	Sec16-like Protein	12	468	0	0	hypothetical protein	-2.21
TGGT1_264090	TRAPPC11	Trafficking protein particle complex subunit 11	2	326.5	0	0	hypothetical protein	-4.74
TGGT1_290310	COG1	Conserved Oligomeric Golgi complex component 1	0	199	0	59	hypothetical protein	-3.75
TGGT1_232190	GBF1	Golgi Brefeldin A resistance guanine nucleotide exchange Factor 1	1	157	0	0	Sec7 domain-containing protein	-5.57
TGGT1_207370	GLP2	Golgi Localizing Protein 2	1	126.5	0	0	hypothetical protein	-3.89
TGGT1_230400	WPDP	WIP-related Protein Domain-containing Protein	2	67	0	0	hypothetical protein	-2.42
TGGT1_216370	GLP3	Golgi Localizing Protein 3	0	46	0	38	hypothetical protein	-4.37
TGGT1_301410	Tepsin	AP-4 complex accessory subunit Tepsin	0	41	0	0	hypothetical protein	-4.16
TGGT1_258080	GLP1	Golgi Localizing Protein 1	0	32.5	0	0	hypothetical protein	-2.41
TGGT1_240220	GLP4	Golgi Localizing Protein 4	0	20	0	0	hypothetical protein	-2.1

657 **Table 1. Summary of Golgi-associated proteins identified in this study.** Table
658 summarizing the twelve novel Golgi-associated proteins identified and characterized in
659 this study, listed in order of enrichment in the ULP1 TurboID experiment. Average spectral
660 counts for each protein in the TurboID and IP experiments are shown ("Ctrl" = control,
661 "Exp" = experimental). GWCS = phenotype score assigned in a genome wide
662 CRISPR/Cas9 screen (33). Abbrv. = protein name abbreviation.
663
664 **Table S1. ULP1 TurboID results.**
665 List of genes identified by mass spectrometry in the ULP1 TurboID experiment. Spectral
666 counts are shown for each gene. "Enrichment Diff" refers to the difference between the
667 average spectral count in ULP1^{TurboID} and control parasites. "Enrichment Fold" refers to
668 the average spectral count for ULP1^{TurboID} samples divided by the average spectral count
669 for control samples. GWCS = phenotype score assigned in a genome wide CRISPR/Cas9
670 screen (33). SP = signal peptide. #TMDs = number of transmembrane domains.
671
672 **Table S2. ULP1 immunoprecipitation results.**
673 List of genes identified by mass spectrometry in the ULP1 immunoprecipitation
674 experiment. Spectral counts are shown for each gene. "Enrichment Diff" refers to the
675 difference between the spectral count in ULP1^{3xHA} IP versus control experiments.
676 "Enrichment Fold" refers to the spectral count for the ULP1^{3xHA} IP sample divided by the
677 spectral count for the control sample. GWCS = phenotype score assigned in a genome
678 wide CRISPR/Cas9 screen (33). SP = signal peptide. #TMDs = number of transmembrane
679 domains.
680
681 **Table S3. Oligonucleotides used in this study.**
682

683 **References**

684 1. Mackintosh CL, Beeson JG, Marsh K. Clinical features and pathogenesis of severe
685 malaria. Trends Parasitol. 2004 Dec;20(12):597–603.

686 2. Sow SO, Muhsen K, Nasrin D, Blackwelder WC, Wu Y, Farag TH, et al. The Burden
687 of Cryptosporidium Diarrheal Disease among Children < 24 Months of Age in
688 Moderate/High Mortality Regions of Sub-Saharan Africa and South Asia, Utilizing
689 Data from the Global Enteric Multicenter Study (GEMS). PLoS Negl Trop Dis. 2016
690 May;10(5):e0004729.

691 3. Sharman PA, Smith NC, Wallach MG, Katrib M. Chasing the golden egg: vaccination
692 against poultry coccidiosis. Parasite Immunol. 2010 Aug;32(8):590–8.

693 4. Kivaria FM. Estimated direct economic costs associated with tick-borne diseases on
694 cattle in Tanzania. Trop Anim Health Prod. 2006 May;38(4):291–9.

695 5. Dubey JP. Review of Neospora caninum and neosporosis in animals. Korean J
696 Parasitol. 2003 Mar;41(1):1–16.

697 6. Pappas G, Roussos N, Falagas ME. Toxoplasmosis snapshots: global status of
698 Toxoplasma gondii seroprevalence and implications for pregnancy and congenital
699 toxoplasmosis. Int J Parasitol. 2009 Oct;39(12):1385–94.

700 7. Tenter AM, Heckeroth AR, Weiss LM. Toxoplasma gondii: from animals to humans.
701 International Journal for Parasitology. 2000 Nov;30(12–13):1217–58.

702 8. Luft BJ, Remington JS. Toxoplasmic Encephalitis in AIDS. Clinical Infectious
703 Diseases. 1992 Aug 1;15(2):211–22.

704 9. Martin S. Congenital Toxoplasmosis. Neonatal Network. 2001 Jun;20(4):23–30.

705 10. Hager KM, Striepen B, Tilney LG, Roos DS. The nuclear envelope serves as an
706 intermediary between the ER and Golgi complex in the intracellular parasite
707 Toxoplasma gondii. J Cell Sci. 1999 Aug;112 (Pt 16):2631–8.

708 11. Tomavo S, Slomianny C, Meissner M, Carruthers VB. Protein trafficking through the
709 endosomal system prepares intracellular parasites for a home invasion. PLoS
710 Pathog. 2013 Oct;9(10):e1003629.

711 12. Joiner KA, Roos DS. Secretory traffic in the eukaryotic parasite Toxoplasma gondii:
712 less is more. J Cell Biol. 2002 May 13;157(4):557–63.

713 13. Gubbels MJ, Duraisingh MT. Evolution of apicomplexan secretory organelles. Int J
714 Parasitol. 2012 Nov;42(12):1071–81.

715 14. Nishi M, Hu K, Murray JM, Roos DS. Organellar dynamics during the cell cycle of
716 Toxoplasma gondii. Journal of Cell Science. 2008 May 1;121(9):1559–68.

717 15. McGovern OL, Rivera-Cuevas Y, Kannan G, Narwold AJ, Carruthers VB.
718 Intersection of endocytic and exocytic systems in Toxoplasma gondii. Traffic. 2018
719 May;19(5):336–53.

720 16. Stasic AJ, Moreno SNJ, Carruthers VB, Dou Z. The Toxoplasma plant-like vacuolar
721 compartment (PLVAC). J Eukaryot Microbiol. 2022 Nov;69(6):e12951.

722 17. Prasad A, Mastud P, Patankar S. Dually localised proteins found in both the
723 apicoplast and mitochondrion utilize the Golgi-dependent pathway for apicoplast
724 targeting in *Toxoplasma gondii*. Biol Cell. 2021 Jan;113(1):58–78.

725 18. Cao S, Yang J, Fu J, Chen H, Jia H. The Dissection of SNAREs Reveals Key
726 Factors for Vesicular Trafficking to the Endosome-like Compartment and Apicoplast
727 via the Secretory System in Toxoplasma gondii. mBio. 2021 Aug 31;12(4):e0138021.

728 19. Miranda K, Pace DA, Cintron R, Rodrigues JCF, Fang J, Smith A, et al.
729 Characterization of a novel organelle in Toxoplasma gondii with similar composition
730 and function to the plant vacuole. Mol Microbiol. 2010 Jun;76(6):1358–75.

731 20. Parussini F, Coppens I, Shah PP, Diamond SL, Carruthers VB. Cathepsin L
732 occupies a vacuolar compartment and is a protein maturase within the endo/exocytic
733 system of Toxoplasma gondii. Mol Microbiol. 2010 Jun;76(6):1340–57.

734 21. Morlon-Guyot J, Pastore S, Berry L, Lebrun M, Daher W. Toxoplasma gondii Vps11,
735 a subunit of HOPS and CORVET tethering complexes, is essential for the
736 biogenesis of secretory organelles. Cell Microbiol. 2015 Aug;17(8):1157–78.

737 22. Sloves PJ, Delhaye S, Mouveaux T, Werkmeister E, Slomianny C, Hovasse A, et al.
738 Toxoplasma sortilin-like receptor regulates protein transport and is essential for
739 apical secretory organelle biogenesis and host infection. Cell Host Microbe. 2012
740 May 17;11(5):515–27.

741 23. Breinich MS, Ferguson DJP, Foth BJ, van Dooren GG, Lebrun M, Quon DV, et al. A
742 dynamin is required for the biogenesis of secretory organelles in Toxoplasma gondii.
743 Curr Biol. 2009 Feb 24;19(4):277–86.

744 24. Klinger CM, Klute MJ, Dacks JB. Comparative genomic analysis of multi-subunit
745 tethering complexes demonstrates an ancient pan-eukaryotic complement and
746 sculpting in Apicomplexa. PLoS One. 2013;8(9):e76278.

747 25. Jimenez-Ruiz E, Morlon-Guyot J, Daher W, Meissner M. Vacuolar protein sorting
748 mechanisms in apicomplexan parasites. Mol Biochem Parasitol. 2016;209(1–2):18–
749 25.

750 26. Chen AL, Kim EW, Toh JY, Vashisht AA, Rashoff AQ, Van C, et al. Novel
751 components of the Toxoplasma inner membrane complex revealed by BioID. Mbio.
752 2015;6(1):e02357-14.

753 27. Sayers EW, Bolton EE, Brister JR, Canese K, Chan J, Comeau DC, et al. Database
754 resources of the national center for biotechnology information. Nucleic Acids Res.
755 2022 Jan 7;50(D1):D20–6.

756 28. Kelley LA, Mezulis S, Yates CM, Wass MN, Sternberg MJE. The Phyre2 web portal
757 for protein modeling, prediction and analysis. Nat Protoc. 2015 Jun;10(6):845–58.

758 29. Heo Y, Yoon HJ, Ko H, Jang S, Lee HH. Crystal structures of Uso1 membrane tether
759 reveal an alternative conformation in the globular head domain. Sci Rep. 2020 Jun
760 12;10(1):9544.

761 30. Paysan-Lafosse T, Blum M, Chuguransky S, Grego T, Pinto BL, Salazar GA, et al.
762 InterPro in 2022. Nucleic Acids Res. 2023 Jan 6;51(D1):D418–27.

763 31. Ludwiczak J, Winski A, Szczepaniak K, Alva V, Dunin-Horkawicz S. DeepCoil-a fast
764 and accurate prediction of coiled-coil domains in protein sequences. Bioinformatics.
765 2019 Aug 15;35(16):2790–5.

766 32. Marsilia C, Batra M, Pokrovskaya ID, Wang C, Chaput D, Naumova DA, et al.
767 Essential role of the conserved oligomeric Golgi complex in Toxoplasma gondii.
768 mBio. 2023 Nov 15;14(6):e0251323.

769 33. Sidik SM, Huet D, Ganesan SM, Huynh MH, Wang T, Nasamu AS, et al. A Genome-
770 wide CRISPR Screen in Toxoplasma Identifies Essential Apicomplexan Genes. Cell.
771 2016;166(6):1423-1435.e12.

772 34. Sidik SM, Hackett CG, Tran F, Westwood NJ, Lourido S. Efficient Genome
773 Engineering of Toxoplasma gondii Using CRISPR/Cas9. Blader IJ, editor. PLoS
774 ONE. 2014 Jun 27;9(6):e100450.

775 35. Shen B, Brown KM, Lee TD, Sibley LD. Efficient Gene Disruption in Diverse Strains
776 of Toxoplasma gondii Using CRISPR/CAS9. Weiss LM, editor. mBio. 2014 May
777 13;5(3):e01114-14.

778 36. Pelletier L, Stern CA, Pypaert M, Sheff D, Ngô HM, Roper N, et al. Golgi biogenesis
779 in Toxoplasma gondii. Nature. 2002 Aug 1;418(6897):548–52.

780 37. Brown KM, Long S, Sibley LD. Conditional Knockdown of Proteins Using Auxin-
781 inducible Degron (AID) Fusions in Toxoplasma gondii. Bio Protoc. 2018 Feb
782 20;8(4):e2728.

783 38. Nishimura K, Fukagawa T, Takisawa H, Kakimoto T, Kanemaki M. An auxin-based
784 degron system for the rapid depletion of proteins in nonplant cells. Nat Methods.
785 2009 Dec;6(12):917–22.

786 39. Back PS, Moon AS, Pasquarelli RR, Bell HN, Torres JA, Chen AL, et al. IMC29
787 Plays an Important Role in Toxoplasma Endodyogeny and Reveals New
788 Components of the Daughter-Enriched IMC Proteome. mBio. 2023 Feb
789 28;14(1):e0304222.

790 40. Beck JR, Rodriguez-Fernandez IA, Cruz de Leon J, Huynh MH, Carruthers VB,
791 Morrissette NS, et al. A Novel Family of Toxoplasma IMC Proteins Displays a
792 Hierarchical Organization and Functions in Coordinating Parasite Division. Soldati-
793 Favre D, editor. PLoS Pathog. 2010 Sep 9;6(9):e1001094.

794 41. Lamarque MH, Roques M, Kong-Hap M, Tonkin ML, Rugarabamu G, Marq JB, et al.
795 Plasticity and redundancy among AMA-RON pairs ensure host cell entry of
796 Toxoplasma parasites. Nat Commun. 2014 Jun 17;5:4098.

797 42. Branon TC, Bosch JA, Sanchez AD, Udeshi ND, Svinkina T, Carr SA, et al. Efficient
798 proximity labeling in living cells and organisms with TurboID. Nat Biotechnol.
799 2018;36(9):880–7.

800 43. Venugopal K, Werkmeister E, Barois N, Saliou JM, Poncet A, Huot L, et al. Dual role
801 of the Toxoplasma gondii clathrin adaptor AP1 in the sorting of rhoptry and
802 microneme proteins and in parasite division. PLoS Pathog. 2017
803 Apr;13(4):e1006331.

804 44. Sakura T, Sindikubwabo F, Oesterlin LK, Bousquet H, Slomianny C, Hakimi MA, et
805 al. A Critical Role for Toxoplasma gondii Vacuolar Protein Sorting VPS9 in Secretory
806 Organelle Biogenesis and Host Infection. Sci Rep. 2016 Dec 14;6:38842.

807 45. Sohda M, Misumi Y, Yoshimura SI, Nakamura N, Fusano T, Ogata S, et al. The
808 interaction of two tethering factors, p115 and COG complex, is required for Golgi
809 integrity. Traffic. 2007 Mar;8(3):270–84.

810 46. Amos B, Aurrecoechea C, Barba M, Barreto A, Basenko EY, Bażant W, et al.
811 VEuPathDB: the eukaryotic pathogen, vector and host bioinformatics resource
812 center. Nucleic Acids Res. 2022 Jan 7;50(D1):D898–911.

813 47. Budnik A, Stephens DJ. ER exit sites - localization and control of COPII vesicle
814 formation. FEBS Lett. 2009 Dec 3;583(23):3796–803.

815 48. Nakajima H, Hirata A, Ogawa Y, Yonehara T, Yoda K, Yamasaki M. A cytoskeleton-
816 related gene, uso1, is required for intracellular protein transport in Saccharomyces
817 cerevisiae. J Cell Biol. 1991 Apr;113(2):245–60.

818 49. Sapperstein SK, Walter DM, Grosvenor AR, Heuser JE, Waters MG. p115 is a
819 general vesicular transport factor related to the yeast endoplasmic reticulum to Golgi
820 transport factor Uso1p. Proc Natl Acad Sci U S A. 1995 Jan 17;92(2):522–6.

821 50. Shorter J, Warren G. A role for the vesicle tethering protein, p115, in the post-mitotic
822 stacking of reassembling Golgi cisternae in a cell-free system. J Cell Biol. 1999 Jul
823 12;146(1):57–70.

824 51. Puthenveedu MA, Linstedt AD. Gene replacement reveals that p115/SNARE
825 interactions are essential for Golgi biogenesis. Proc Natl Acad Sci U S A. 2004 Feb
826 3;101(5):1253–6.

827 52. Noda Y, Yamagishi T, Yoda K. Specific membrane recruitment of Uso1 protein, the
828 essential endoplasmic reticulum-to-Golgi tethering factor in yeast vesicular transport.
829 J Cell Biochem. 2007 Jun 1;101(3):686–94.

830 53. Bravo-Plaza I, Tagua VG, Arst HN, Alonso A, Pinar M, Monterroso B, et al. The
831 Uso1 globular head interacts with SNAREs to maintain viability even in the absence
832 of the coiled-coil domain. Elife. 2023 May 30;12:e85079.

833 54. Kim S, Hill A, Warman ML, Smits P. Golgi disruption and early embryonic lethality in
834 mice lacking USO1. PLoS One. 2012;7(11):e50530.

835 55. Radulescu AE, Mukherjee S, Shields D. The Golgi protein p115 associates with
836 gamma-tubulin and plays a role in Golgi structure and mitosis progression. J Biol
837 Chem. 2011 Jun 17;286(24):21915–26.

838 56. Ibar C, Glavic Á. Drosophila p115 is required for Cdk1 activation and G2/M cell cycle
839 transition. Mech Dev. 2017 Apr;144(Pt B):191–200.

840 57. Allan BB, Moyer BD, Balch WE. Rab1 recruitment of p115 into a cis-SNARE
841 complex: programming budding COPII vesicles for fusion. Science. 2000 Jul
842 21;289(5478):444–8.

843 58. García-Mata R, Sztul E. The membrane-tethering protein p115 interacts with GBF1,
844 an ARF guanine-nucleotide-exchange factor. EMBO Rep. 2003 Mar;4(3):320–5.

845 59. Nakamura N, Lowe M, Levine TP, Rabouille C, Warren G. The vesicle docking
846 protein p115 binds GM130, a cis-Golgi matrix protein, in a mitotically regulated
847 manner. Cell. 1997 May 2;89(3):445–55.

848 60. Sano R, Reed JC. ER stress-induced cell death mechanisms. Biochim Biophys Acta.
849 2013 Dec;1833(12):3460–70.

850 61. Salama NR, Chuang JS, Schekman RW. Sec31 encodes an essential component of
851 the COPII coat required for transport vesicle budding from the endoplasmic
852 reticulum. Mol Biol Cell. 1997 Feb;8(2):205–17.

853 62. Hu H, Gourguechon S, Wang CC, Li Z. The G1 Cyclin-dependent Kinase CRK1 in
854 Trypanosoma brucei Regulates Anterograde Protein Transport by Phosphorylating
855 the COPII Subunit Sec31. J Biol Chem. 2016 Jul 22;291(30):15527–39.

856 63. Claude A, Zhao BP, Kuziemsky CE, Dahan S, Berger SJ, Yan JP, et al. GBF1: A
857 novel Golgi-associated BFA-resistant guanine nucleotide exchange factor that
858 displays specificity for ADP-ribosylation factor 5. J Cell Biol. 1999 Jul 12;146(1):71–
859 84.

860 64. Szul T, Grabski R, Lyons S, Morohashi Y, Shestopal S, Lowe M, et al. Dissecting the
861 role of the ARF guanine nucleotide exchange factor GBF1 in Golgi biogenesis and
862 protein trafficking. J Cell Sci. 2007 Nov 15;120(Pt 22):3929–40.

863 65. Blackburn JB, D'Souza Z, Lupashin VV. Maintaining order: COG complex controls
864 Golgi trafficking, processing, and sorting. FEBS Lett. 2019 Sep;593(17):2466–87.

865 66. Smith RD, Lupashin VV. Role of the conserved oligomeric Golgi (COG) complex in
866 protein glycosylation. Carbohydr Res. 2008 Aug 11;343(12):2024–31.

867 67. Fauquenoy S, Hovasse A, Sloves PJ, Morelle W, Dilezitoko Alayi T, Slomianny C, et
868 al. Unusual N-glycan structures required for trafficking Toxoplasma gondii GAP50 to
869 the inner membrane complex regulate host cell entry through parasite motility. Mol
870 Cell Proteomics. 2011 Sep;10(9):M111.008953.

871 68. Tomita T, Sugi T, Yakubu R, Tu V, Ma Y, Weiss LM. Making Home Sweet and
872 Sturdy: Toxoplasma gondii ppGalNAc-Ts Glycosylate in Hierarchical Order and
873 Confer Cyst Wall Rigidity. mBio. 2017 Jan 10;8(1):e02048-16.

874 69. Borner GHH, Antrobus R, Hirst J, Bhumbra GS, Kozik P, Jackson LP, et al.
875 Multivariate proteomic profiling identifies novel accessory proteins of coated
876 vesicles. J Cell Biol. 2012 Apr 2;197(1):141–60.

877 70. Wallace NS, Gadbery JE, Cohen CI, Kendall AK, Jackson LP. Tepsin binds LC3B to
878 promote ATG9A export and delivery at the cell periphery. bioRxiv. 2023 Jul
879 18;2023.07.18.549521.

880 71. Scrivens PJ, Noueihed B, Shahrzad N, Hul S, Brunet S, Sacher M. C4orf41 and
881 TTC-15 are mammalian TRAPP components with a role at an early stage in ER-to-
882 Golgi trafficking. Mol Biol Cell. 2011 Jun 15;22(12):2083–93.

883 72. Whittle JRR, Schwartz TU. Structure of the Sec13-Sec16 edge element, a template
884 for assembly of the COPII vesicle coat. J Cell Biol. 2010 Aug 9;190(3):347–61.

885 73. Bharucha N, Liu Y, Papanikou E, McMahon C, Esaki M, Jeffrey PD, et al. Sec16
886 influences transitional ER sites by regulating rather than organizing COPII. Mol Biol
887 Cell. 2013 Nov;24(21):3406–19.

888 74. Zhang M, Wang C, Otto TD, Oberstaller J, Liao X, Adapa SR, et al. Uncovering the
889 essential genes of the human malaria parasite Plasmodium falciparum by saturation
890 mutagenesis. Science. 2018 May 4;360(6388):eaap7847.

891 75. Egea G, Serra-Peinado C, Gavilan MP, Rios RM. Cytoskeleton and Golgi-apparatus
892 interactions: a two-way road of function and structure. CHC. 2015 Jan;37.

893 76. Munro S. The golgin coiled-coil proteins of the Golgi apparatus. Cold Spring Harb
894 Perspect Biol. 2011 Jun 1;3(6):a005256.

895 77. Donald RG, Roos DS. Stable molecular transformation of Toxoplasma gondii: a
896 selectable dihydrofolate reductase-thymidylate synthase marker based on drug-
897 resistance mutations in malaria. Proc Natl Acad Sci U S A. 1993 Dec
898 15;90(24):11703–7.

899 78. Kim K, Soldati D, Boothroyd JC. Gene replacement in Toxoplasma gondii with
900 chloramphenicol acetyltransferase as selectable marker. Science. 1993 Nov
901 5;262(5135):911–4.

902 79. Donald RG, Carter D, Ullman B, Roos DS. Insertional tagging, cloning, and
903 expression of the Toxoplasma gondii hypoxanthine-xanthine-guanine
904 phosphoribosyltransferase gene: Use as a selectable marker for stable
905 transformation. J Biol Chem. 1996 Jun 14;271(24):14010–9.

906 80. Choi CP, Moon AS, Back PS, Jami-Alahmadi Y, Vashisht AA, Wohlschlegel JA, et
907 al. A photoactivatable crosslinking system reveals protein interactions in the
908 Toxoplasma gondii inner membrane complex. PLOS Biology. 2019 Oct
909 4;17(10):e3000475.

910 81. Francia ME, Wicher S, Pace DA, Sullivan J, Moreno SNJ, Arrizabalaga G. A
911 Toxoplasma gondii protein with homology to intracellular type Na^+/H^+ exchangers is
912 important for osmoregulation and invasion. Exp Cell Res. 2011 Jun
913 10;317(10):1382–96.

914 82. Nagamune K, Beatty WL, Sibley LD. Artemisinin induces calcium-dependent protein
915 secretion in the protozoan parasite Toxoplasma gondii. Eukaryot Cell. 2007
916 Nov;6(11):2147–56.

917 83. Rome ME, Beck JR, Turetzky JM, Webster P, Bradley PJ. Intervacuolar transport
918 and unique topology of GRA14, a novel dense granule protein in Toxoplasma gondii.
919 Infect Immun. 2008 Nov;76(11):4865–75.

920 84. Carruthers VB, Sherman GD, Sibley LD. The Toxoplasma adhesive protein MIC2 is
921 proteolytically processed at multiple sites by two parasite-derived proteases. J Biol
922 Chem. 2000 May 12;275(19):14346–53.

923 85. DeRocher AE, Coppens I, Karnataki A, Gilbert LA, Rome ME, Feagin JE, et al. A
924 thioredoxin family protein of the apicoplast periphery identifies abundant candidate
925 transport vesicles in Toxoplasma gondii. Eukaryot Cell. 2008 Sep;7(9):1518–29.

926 86. Frénal K, Marq JB, Jacot D, Polonais V, Soldati-Favre D. Plasticity between MyoC-
927 and MyoA-glideosomes: an example of functional compensation in Toxoplasma
928 gondii invasion. PLoS Pathog. 2014 Oct;10(10):e1004504.

929 87. Bradley PJ, Ward C, Cheng SJ, Alexander DL, Coller S, Coombs GH, et al.
930 Proteomic Analysis of Rhoptry Organelles Reveals Many Novel Constituents for
931 Host-Parasite Interactions in Toxoplasma gondii. Journal of Biological Chemistry.
932 2005 Oct;280(40):34245–58.

933 88. Huynh MH, Carruthers VB. Tagging of endogenous genes in a Toxoplasma gondii
934 strain lacking Ku80. Eukaryot Cell. 2009 Apr;8(4):530–9.

935 89. Bradley PJ, Rayatpisheh S, Wohlschlegel JA, Nadipuram SM. Using BioID for the
936 Identification of Interacting and Proximal Proteins in Subcellular Compartments in
937 Toxoplasma gondii. Methods Mol Biol. 2020;2071:323–46.

938 90. Xu T, Park SK, Venable JD, Wohlschlegel JA, Diedrich JK, Cociorva D, et al.
939 ProLuCID: An improved SEQUEST-like algorithm with enhanced sensitivity and
940 specificity. Journal of Proteomics. 2015 Nov 3;129:16–24.

941 91. Tabb DL, McDonald WH, Yates JR. DTASelect and Contrast: Tools for Assembling
942 and Comparing Protein Identifications from Shotgun Proteomics. J Proteome Res.
943 2002 Feb 1;1(1):21–6.

944 92. Cociorva D, L. Tabb D, Yates JR. Validation of Tandem Mass Spectrometry
945 Database Search Results Using DTASelect. Current Protocols in Bioinformatics.
946 2006;16(1):13.4.1-13.4.14.

947 93. Florens L, Carozza MJ, Swanson SK, Fournier M, Coleman MK, Workman JL, et al.
948 Analyzing chromatin remodeling complexes using shotgun proteomics and
949 normalized spectral abundance factors. Methods. 2006 Dec 1;40(4):303–11.

950 94. Mistry J, Chuguransky S, Williams L, Qureshi M, Salazar GA, Sonnhammer ELL, et
951 al. Pfam: The protein families database in 2021. Nucleic Acids Res. 2021 Jan
952 8;49(D1):D412–9.

953 95. Thomas PD, Ebert D, Muruganujan A, Mushayahama T, Albou LP, Mi H. PANTHER:
954 Making genome-scale phylogenetics accessible to all. Protein Sci. 2022
955 Jan;31(1):8–22.

956